Supporting Information

Contribution of microorganisms with the Clade II nitrous oxide reductase to suppression of surface emissions of nitrous oxide

Kristopher A. Hunt, Alex V. Carr, Anne E. Otwell, Jacob J. Valenzuela, Kathleen S. Walker, Emma R. Dixon, Lauren M. Lui, Torben Nielsen, Samuel Bowman, Frederick von Netzer, Ji-Won Moon, Christopher W. Schadt, Miguel Rodriguez Jr., Kenneth Lowe, Dominique Joyner, Katherine J. Davis, Xiaoqin Wu, Romy Chakraborty, Matthew W. Fields, Jizhong Zhou, Terry C. Hazen, Adam P. Arkin, Scott D. Wankel, Nitin Baliga, and David A. Stahl

Description of Supporting Information (13 pages, 3 tables, 9 figures)

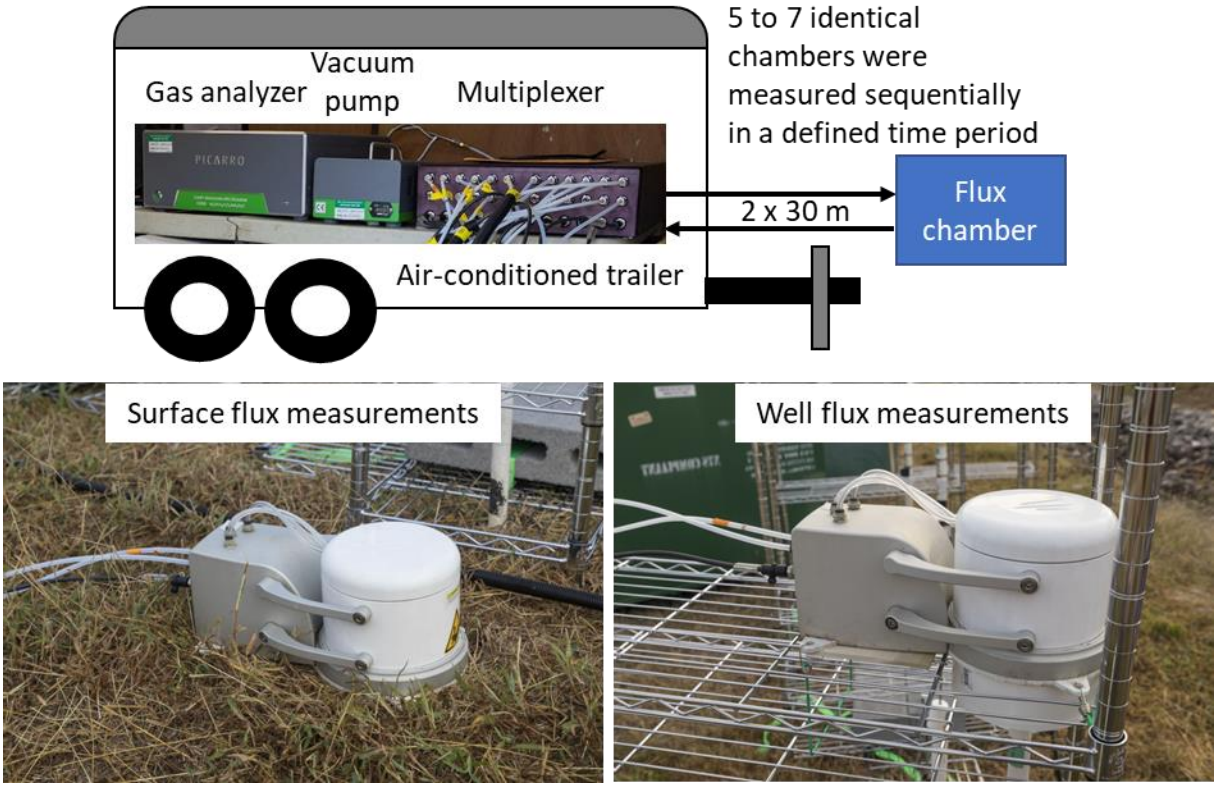

Figure S1. Instrumentation for flux measurements. Measurements were made using a Picarro gas analyzer and Eosense automated flux chambers. The equipment was protected from field conditions by an air-conditioned trailer with an opening for connection to the automated flux chambers distributed around the area. Chambers were connected to the Eosense multiplexer unit via 30 m lines and cables. The chamber used for surface measurements had an area of 0.018 m^2 and a volume of 2892 ml.

Table S1. Physical characteristics of wells and adapters used for flux monitoring.

Location	Well inner diameter (m)	Chamber volume (ml)	Screened region	
			Meters to top	Meters to bottom
SG012	0.021	2548	0.44	1.90
SG010	0.021	2548	1.25	2.08
SG004	0.021	2548	2.38	2.93
SG002	0.021	2548	1.89	2.96
FW116	0.043	2548	3.72	5.18
FW117	0.043	2548	6.00	7.46

Table S2. Flux measurement sequencing.

Chamber	Well	Defined cycle	Pre-valve (min)	Post-valve (min)	Closed (min)	Start Date Time
1	SG004	1	180	180	3180	2019-09-23 19:15
2	SG010	1	180	180	3180	2019-09-23 19:15
3	FW117	1	180	180	3180	2019-09-23 19:15
4	FW116	1	180	180	3180	2019-09-23 19:15
5	SG012	1	180	180	3180	2019-09-23 19:15
6	SG002	1	180	180	3180	2019-09-23 19:15
1	SG010	2	180	180	3180	2019-09-27 08:25
2	SG004	2	180	180	3180	2019-09-27 08:25
3	FW116	2	180	180	3180	2019-09-27 08:25
4	FW117	2	180	180	3180	2019-09-27 08:25
5	SG002	2	180	180	3180	2019-09-27 08:25
6	SG012	2	180	180	3180	2019-09-27 08:25
1	SG004	3	180	180	1500	2019-09-27 19:15
2	SG010	3	180	180	900	2019-09-27 19:15
3	FW117	3	180	180	1500	2019-09-27 19:15
4	FW116	3	180	180	1500	2019-09-27 19:15
5	SG012	3	180	180	1500	2019-09-27 19:15
6	SG002	3	180	180	1500	2019-09-27 19:15
1	SG004	4	180	180	900	2019-10-07 16:45
2	SG010	4	180	180	600	2019-10-07 16:45
3	FW117	4	180	180	900	2019-10-07 16:45
4	FW116	4	180	180	900	2019-10-07 16:45
5	SG012	4	180	180	900	2019-10-07 16:45
6	SG002	4	180	180	900	2019-10-07 16:45
9	Surface 3	4	180	180	900	2019-10-07 16:45
11	Surface 5	4	180	180	900	2019-10-07 16:45
12	Surface 1	4	180	180	900	2019-10-07 16:45
1	SG004	5	180	180	900	2019-10-09 16:15
2	SG010	5	180	180	600	2019-10-09 16:15
3	FW117	5	180	180	900	2019-10-09 16:15
4	FW116	5	180	180	900	2019-10-09 16:15
5	SG012	5	180	180	900	2019-10-09 16:15
6	SG002	5	180	180	900	2019-10-09 16:15
9	Surface 3	5	180	180	900	2019-10-09 16:15
12	Surface 5	5	180	180	900	2019-10-09 16:15
1	Surface 1	6	180	180	900	2019-10-14 06:00
2	SG010	6	180	180	600	2019-10-14 06:00
3	FW117	6	180	180	900	2019-10-14 06:00
4	FW116	6	180	180	900	2019-10-14 06:00
6	Surface 4	6	180	180	900	2019-10-14 06:00
9	Surface 3	6	180	180	900	2019-10-14 06:00
11	Surface 2	6	180	180	900	2019-10-14 06:00
12	Surface 5	6	180	180	900	2019-10-14 06:00

Table S3. Metagenome statistics from 2017 core sediment sampling.

Sample ID	Well	Total number of contigs	Average coverage	Number of Gbases	Total reads mapped	Depth of core (m)
EB106-02-01	EB106	1293886	17.40	16.56	1.40E+08	0.91-1.14
EB106-02-02	EB106	2181819	16.05	28.25	2.32E+08	1.14-1.37
EB106-02-03	EB106	871439	28.85	25.25	1.95E+08	1.37-1.5
EB106-03-01	EB106	208626	99.45	31.47	2.31E+08	1.83-1.98
EB106-03-02	EB106	144405	239.92	25.98	1.87E+08	1.98-2.12
EB106-03-03	EB106	382311	25.17	7.65	6.46E+07	2.12-2.27
EB106-03-04	EB106	318027	34.00	6.20	5.11E+07	2.27-2.42
EB106-03-05	EB106	510572	11.13	3.18	3.88E+07	2.42-2.56
EB106-04-01	EB106	421409	15.40	3.05	3.62E+07	2.74-2.91
EB106-04-04	EB106	6209	2621.18	16.69	1.23E+08	3.26-3.43
EB271-02-01	EB271	2002218	14.10	23.72	1.96E+08	0.91-1.14
EB271-02-02	EB271	1742386	15.79	23.87	1.91E+08	1.14-1.37
EB271-02-03	EB271	1829402	10.50	13.36	1.22E+08	1.37-1.47
EB271-03-01	EB271	4370420	10.10	30.70	2.66E+08	1.83-2.06
EB271-03-02	EB271	3596980	10.88	28.54	2.42E+08	2.06-2.29
EB271-03-03	EB271	1787737	15.98	22.95	1.82E+08	2.29-2.57
EB271-04-01	EB271	1323569	22.43	26.37	1.98E+08	2.74-2.97
EB271-04-02	EB271	1893841	17.55	27.52	2.14E+08	2.97-3.2
EB271-04-03	EB271	2605951	9.91	17.68	1.55E+08	3.2-3.43

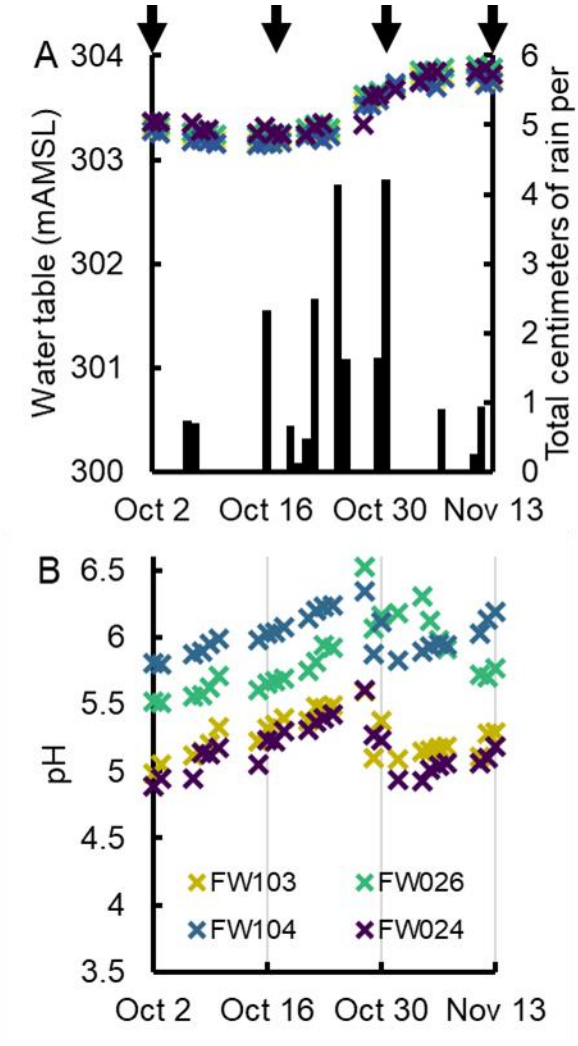

Figure S2. Influence of rain on water table and pH. A dry period during the months leading up to sampling (less than 0.5 cm of rain per day) was followed by a rain event that restored the water table (A) and coincided with a drop in pH (B).

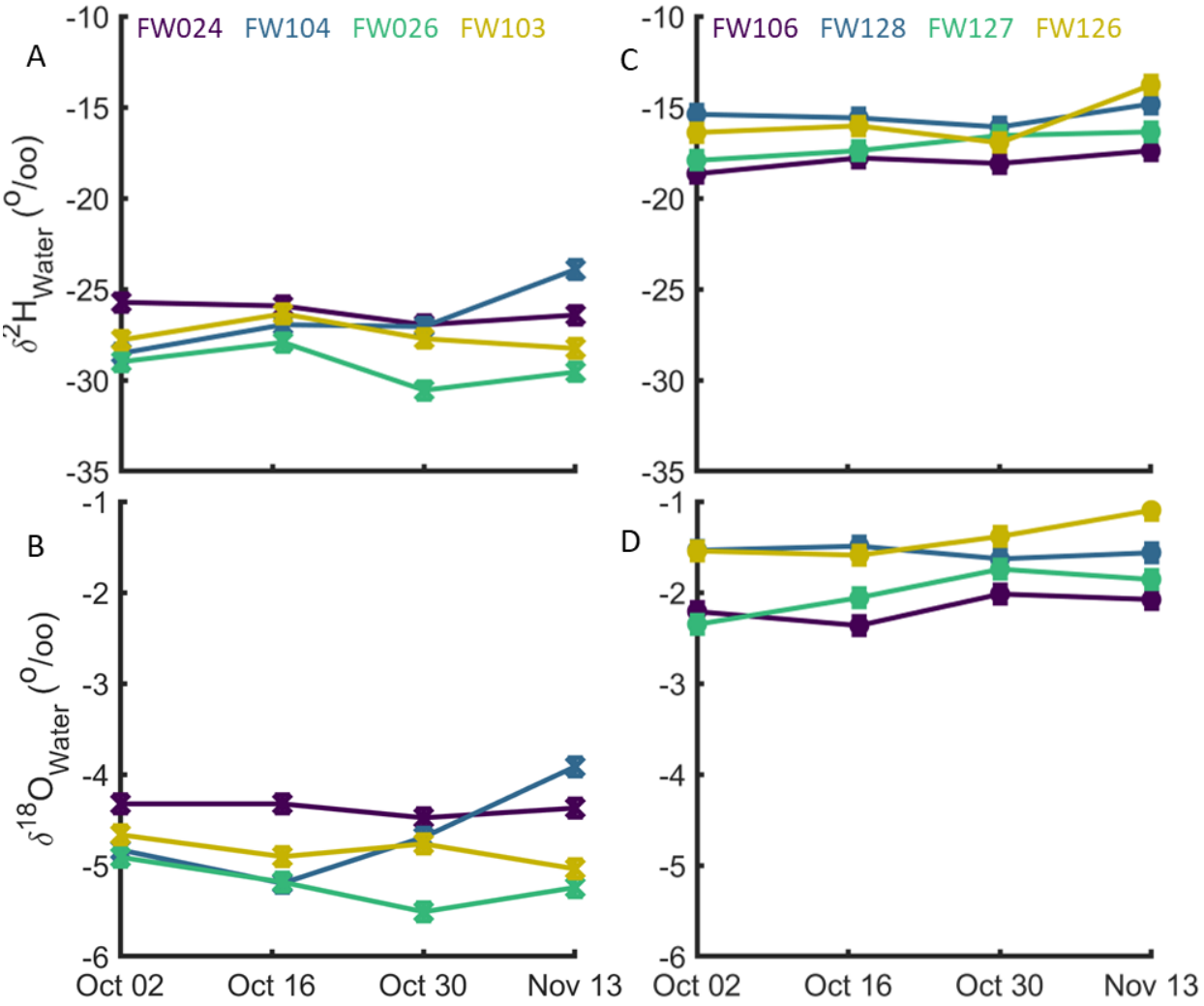

Figure S3. Temporal shifts in groundwater δ^2H and $\delta^{18}O$. Isotopic composition of groundwater collected from different wells was relatively constant across time but distinct between the two groups of wells (A and B compared to C and D).

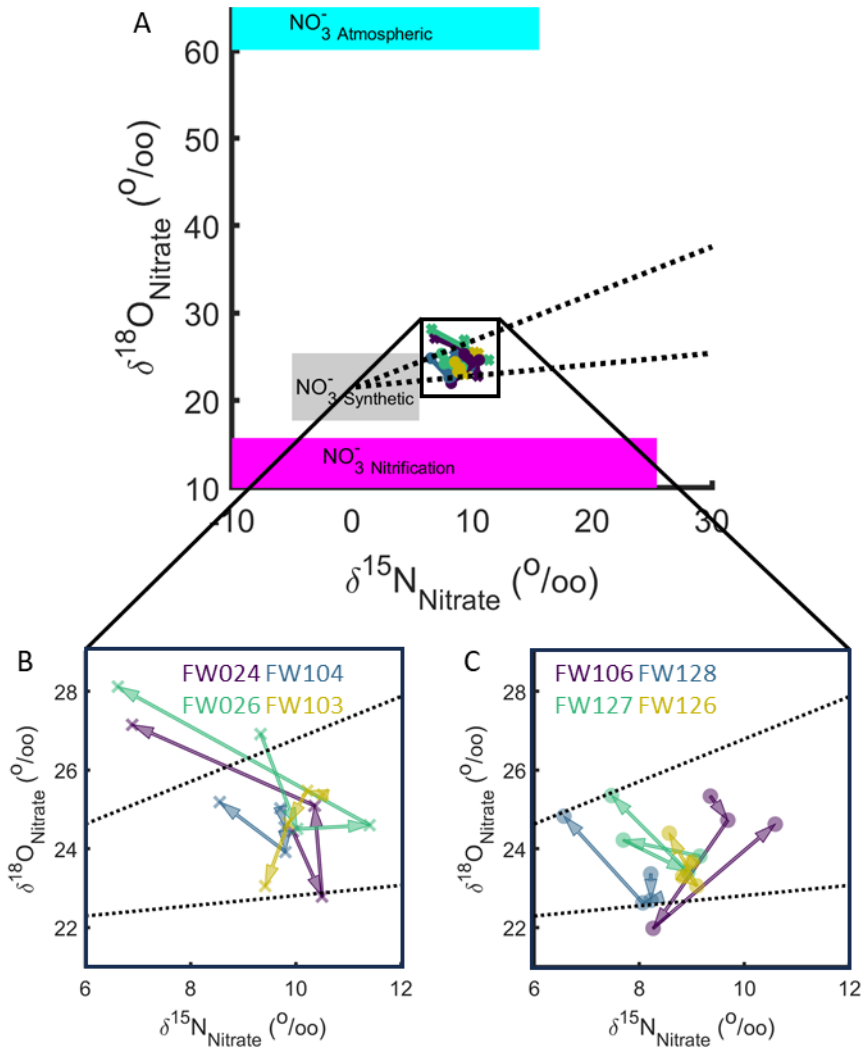

Figure S4. Temporal shifts in isotopic composition of nitrate. The nitrate contamination of the former S3 ponds is synthetic in origin (gray shaded region) (A). While this source nitrate is not available for isotopic characterization, the elevated $\delta^{18}O$ and $\delta^{15}N$ values of nitrate in the sampled wells indicate the nitrate pool from the S3 ponds has undergone denitrification, as indicated by compositions within the range of reported trajectories of a denitrified synthetic nitrate source (black dotted lines). Nitrate from nitrification or rain would be expected to fall in the regions shaded magenta and cyan, respectively. Arrows in the inset graphs show changes in isotopic composition with time (B and C). Typical reproducibility for $\delta^{15}N$ was +/- 0.3‰ and for $\delta^{18}O$ is +/- 0.4‰.

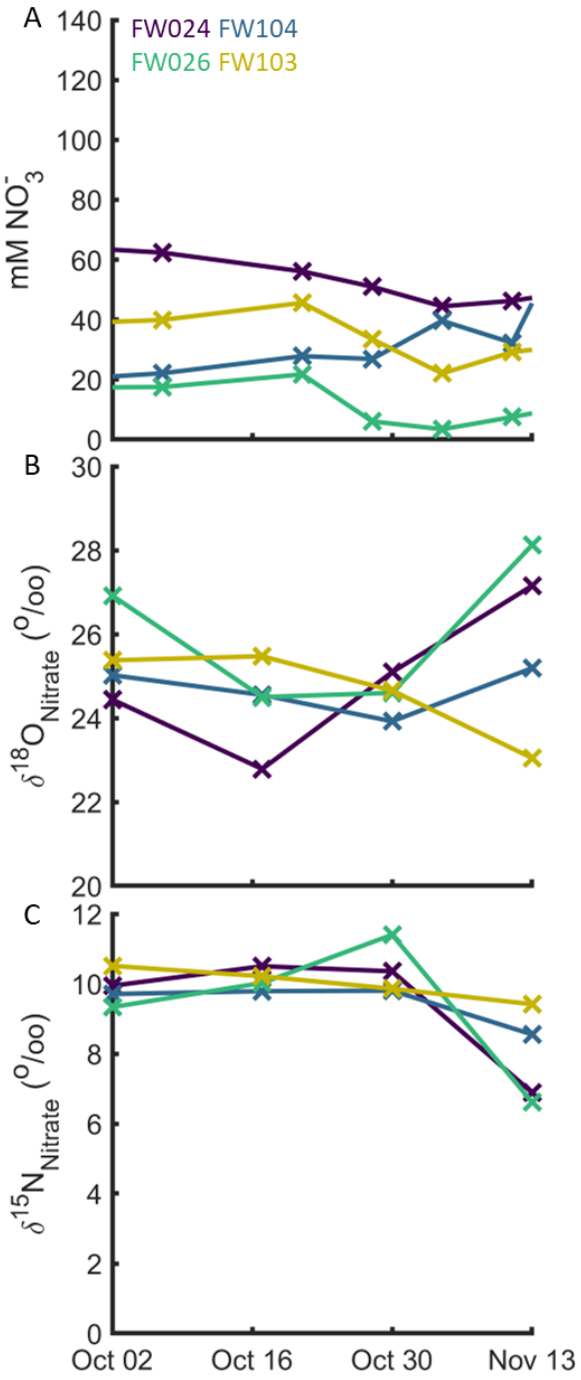

Figure S5. Temporal variation in nitrate isotopic compositions. Isotopic composition for individual wells was relatively constant through time, indicating minor perturbations of process or transport, with notable exceptions. In FW104 and FW024, nitrate concentration (A) decreased near the time of the rain events, Oct 16-30. While FW024 may have been recharged with a less reduced source of nitrate causing the $\delta^{18}O$ and $\delta^{15}N$ values to decrease, this alone does not account for the separation of $\delta^{18}O$ and $\delta^{15}N$ signals with increasing $\delta^{18}O$ and decreasing $\delta^{15}N$. While nitrite oxidizing bacteria did increase in abundance during the rain events, they were less than 0.1% of total population (Figure S6).

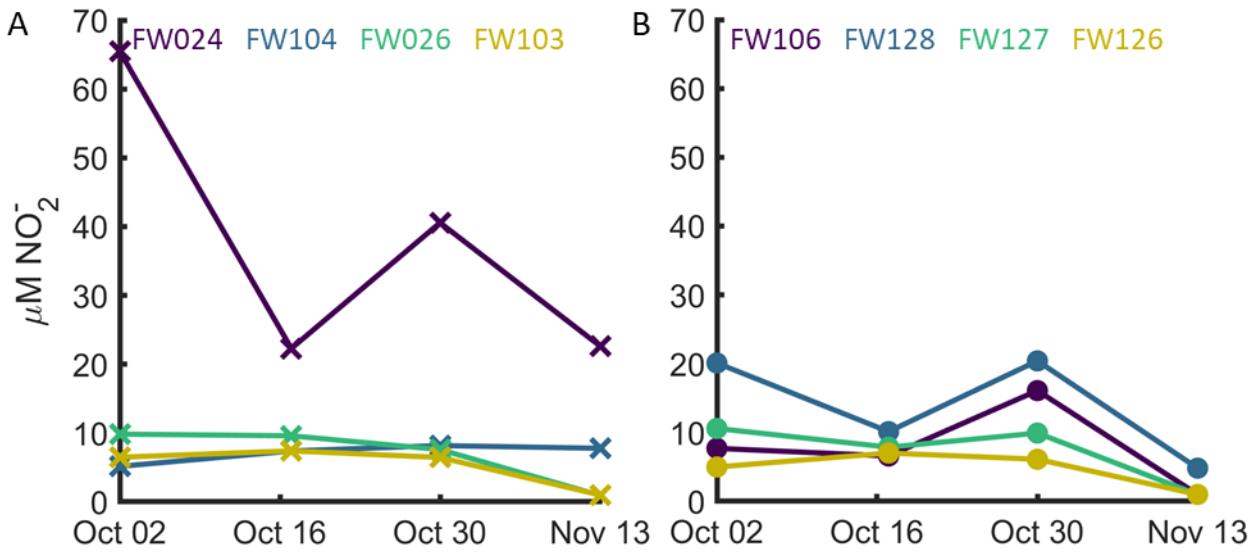

Figure S6. Nitrite concentrations were relatively consistent over the course of the sampling campaign approaching the limit of detection after the rain event (Oct 16-30, 2019). Panels A and B correspond with wells in Figure 1 marked with X's and circles, respectively.

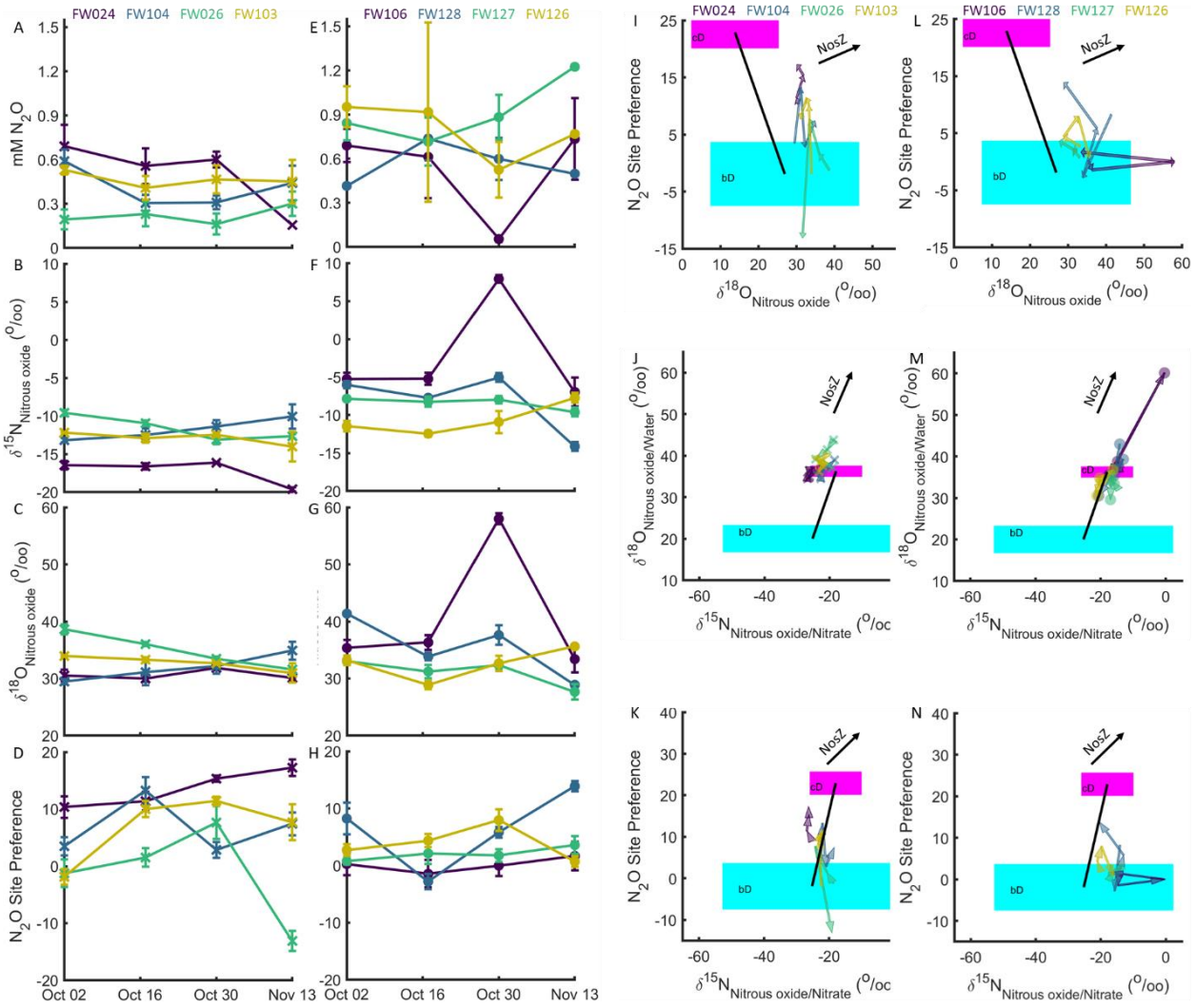

Figure S7. Site specific temporal shifts in nitrous oxide reduction tracked by changes in concentration and isotopic composition. Changes in concentration (A and E) as well as $\delta^{15}N$ (B and F) and $\delta^{18}O$ (C and G) composition of nitrous oxide indicate shifting reduction activity over time. Nitrous oxide site preference and enrichment in ^{18}O (D and H) are consistent with both a mixed biotic-abiotic source and consumption through biotic reduction. The solid black line connecting the regions of chemodenitrification and bacterial denitrification (I-N) is the mixing line for a linear combination of bacterial denitrification (bD, cyan box) and chemodenitrification (cD, magenta box). The range of observed values of $\delta^{18}O$ was much larger without normalization by the $\delta^{18}O$ of the water yet all wells are to the right of the mixing line, supporting nitrous oxide reduction. The impact of biotic nitrous oxide reduction on the nitrous oxide pool is enrichment in both $\delta^{18}O$ and $\delta^{15}N$, as shown by the black arrow labeled NosZ (I-N). Error bars show standard deviations of at most triplicate technical replicates. Colored arrows indicate differences between sampling time points (L-N).

Section S1. *Normalizing isotopic signals to remove environment specific effects.* As described by Yu *et. al.* 2020, $\delta^{15}N$ and $\delta^{18}O$ were normalized by the expected source nitrate and water, respectively, to remove environmental specific effects, including unusual nitrate isotopic compositions and equilibration of the oxygens in nitrite with water. This normalization used the ratio of the heavy and light isotopic components, assuming reference contributions were relatively similar for all measured species.

$$(1) \qquad \delta^{15}N_{\frac{Nitrous\ oxide}{Nitrate}} = \frac{R_{Nitrous\ oxide}}{R_{Nitrate}} = \left(\frac{\left(\frac{\delta^{15}N_{Nitrous\ oxide}}{1000} + 1 \right)}{\frac{\delta^{15}N_{Nitrate}}{1000} + 1} - 1 \right) 1000$$

$$(2) \qquad \delta^{18}O_{\frac{Nitrous\ oxide}{Water}} = \frac{R_{Nitrous\ oxide}}{R_{Water}} = \left(\frac{\left(\frac{\delta^{18}O_{Nitrous\ oxide}}{1000} + 1 \right)}{\frac{\delta^{18}O_{Water}}{1000} + 1} - 1 \right) 1000$$

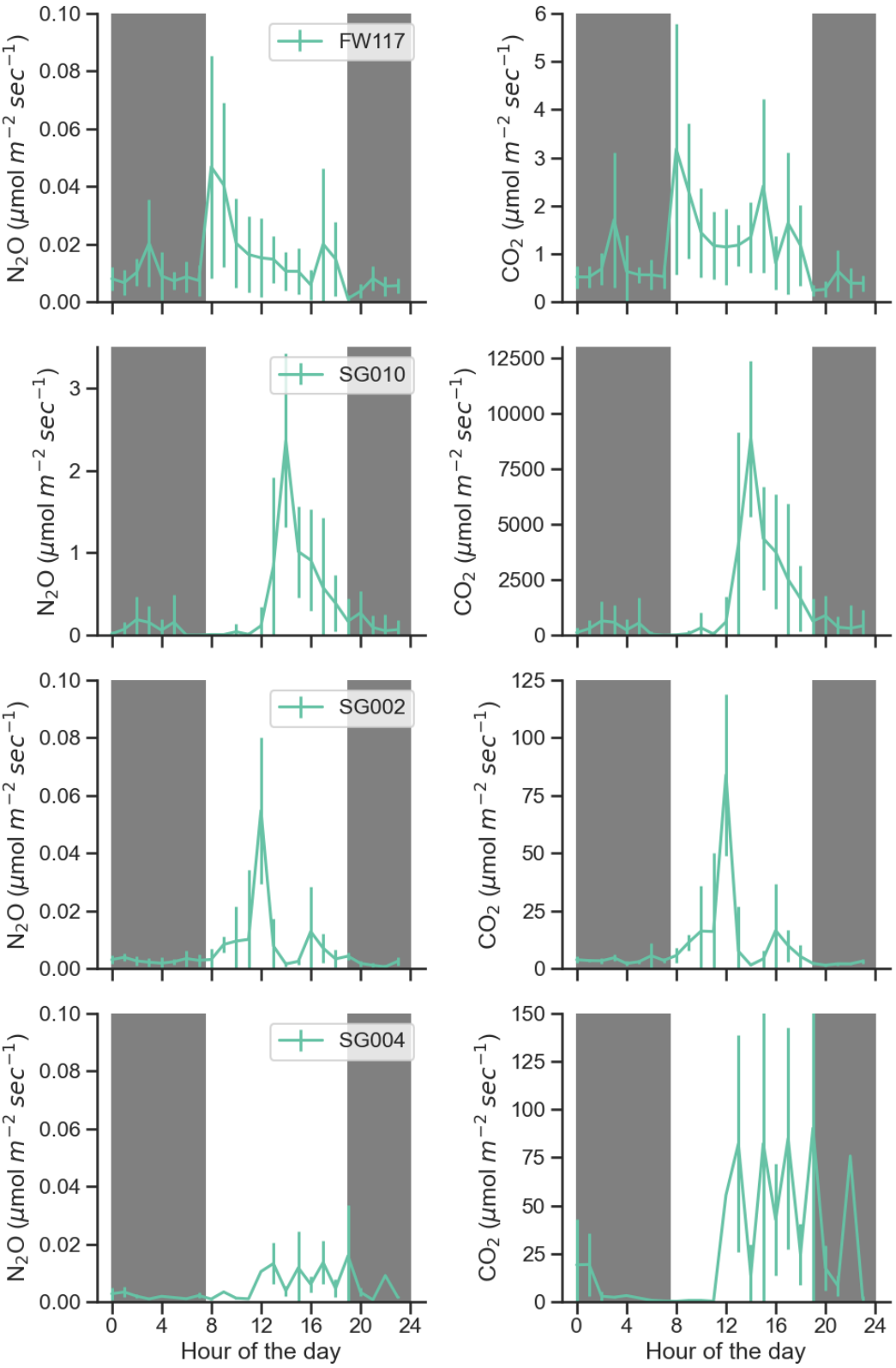

Figure S8. Emissions of nitrous oxide and carbon dioxide were elevated during the daytime hours.

Section S2. *Diffusion based correction of flux through soil and sediment.* The measured nitrous oxide and carbon dioxide flux from wells is an upper limit of flux from the screened depth due to the resistance of gas diffusion through soil and sediment. Measured well fluxes were adjusted to inferred sediment fluxes to account for this transport limitation, using an average sediment porosity for clay, sand, and gravel of 0.2 to estimate a relative sediment diffusion coefficient D_{soil}/D_{air} of 0.03[45]. The concentration gradient in the sediment can decrease or increase due to production or consumption, respectively. However, surface flux of nitrous oxide was generally below the limit of detection of the instrument (0.001 μmol m^{-2} sec^{-1}) supporting a concentration gradient at least as large as that observed from the corresponding well. Holding the concentration gradient and range of that gradient as constant, the flux was adjusted for the slower diffusion using equation 3 (Figure S9). The resulting inferred nitrous oxide sediment fluxes aligned with the reported surface measurements; however, these surface measurements may be overestimated since they were below the limit of detection for the instrument configuration.

(3) $$Inferred\ soil\ flux = Measured\ well\ flux * D_{soil}/D_{air}$$

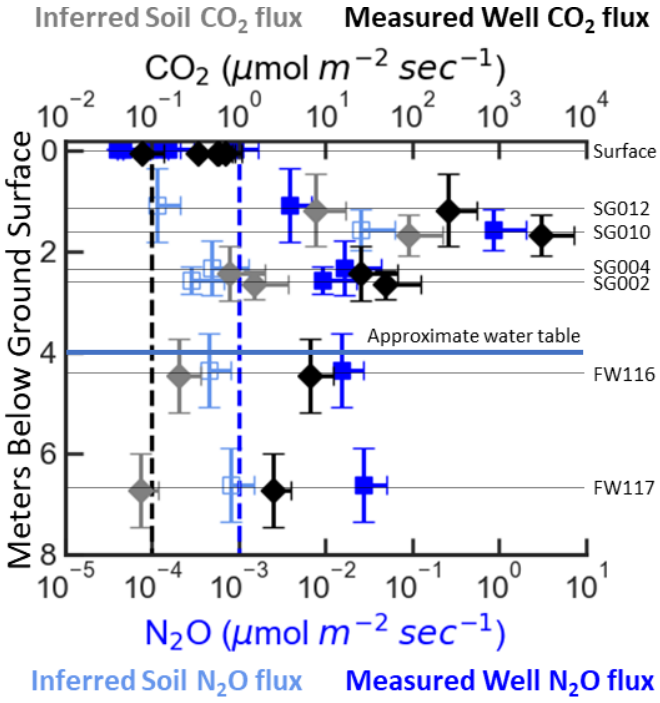

Figure S9. Nitrous oxide and carbon dioxide flux at the surface and from wells screened at different depths. Measured nitrous oxide and carbon dioxide fluxes, determined from at least 11 measurements from each well (Sept 22-27, 2019) support significant metabolic and respiratory activity in the vadose zone. The flux measurements represent an upper limit of the flux possible through the subsurface and were corrected for the relative diffusion coefficient of a gas through sediment (lighter colored symbols). All surface measurements and the limits of detection for surface measurements (dashed lines) are plotted to highlight that slower diffusion in the deeper sediment column may be decreasing the flux of carbon dioxide through the sediment as discussed in the main text.